Available online at www.sciencedirect.com
ScienceDirect
Acta Biomaterialia 5 (2009) 3295–3304
Acta BIOMATERIALIA
www.elsevier.com/locate/actabiomat

Development of an electrospun nano-apatite/PCL composite membrane for GTR/GBR application

Fang Yang [a], Sanne K. Both [a], Xuechao Yang [a,b], X. Frank Walboomers [a], John A. Jansen [a,*]

[a] Department of Periodontology and Biomaterials, Radboud University Nijmegen Medical Center, Nijmegen, The Netherlands
[b] Key Lab for Oral Biomedical Engineering of Ministry of Education and Department of Endodontics, School and Hospital of Stomatology, Wuhan University, 237 Luoyu Road, 430079 Wuhan, Hubei Province, China

Received 20 November 2008; received in revised form 5 March 2009; accepted 14 May 2009
Available online 24 May 2009

Abstract

In dental practice, membranes are used as a barrier to prevent soft tissue ingrowth and create space for slowly regenerating periodontal and bony tissues. The aim of this study was to develop a biodegradable membrane system which can be used for guided tissue or bone regeneration. Three types of composite fibrous membranes based on nano-apatite (nAp) and poly(ε-caprolactone) (PCL) were made by electrospinning, i.e. n0 (nAp:PCL = 0:100), n25 (nAp:PCL = 25:100) and n50 (nAp:PCL = 50:100) with average fiber diameters ranging from 320 to 430 nm. Their structural, mechanical, chemical and biological properties were evaluated. Tensile test revealed that n25 had the highest strength and toughness, indicating there is an optimal ratio of nAp to polymer for mechanical reinforcement. Subsequently, a simulated body fluid immersion test confirmed that the presence of nAp enhanced the bioactive behavior of the membranes. Finally, an in vitro osteoblast cell study showed that all membranes supported proliferation, but the presence of nAp facilitated an early cell differentiation. This study demonstrated that an electrospun membrane incorporating nAp is strong, enhances bioactivity and supports osteoblast-like cell proliferation and differentiation. The membrane system can be used as a prototype for the further development of an optimal membrane for clinical use.

Keywords: Nano-apatite; Poly(ε-caprolactone); Electrospinning; Rat bone marrow cells; Guided tissue regeneration

1. Introduction

In dentistry the concept of guided tissue regeneration (GTR) is frequently applied in reconstruction of periodontal defects, i.e. an occlusive membrane is used to prevent the faster-growing connective tissue from migrating into the defect and to allow time for periodontal ligament, cementum and bone to reconstruct [1]. Similar to GTR, the concept of guided bone regeneration (GBR) is applied at dental implant sites where a membrane is used to cover the bone defect to encourage new bone ingrowth while preventing the ingrowth of fibrous tissue into the grafted site [2,3].

In general, the commercially available GTR/GBR membranes are made of polymers, including non-degradable polytetrafluoroethylene (PTFE: Gore-Tex® (W.L. Gore & Associates, Inc., Elkton, MD, USA)) and TefGen® (Lifecore Biomedical, LLC, Chaska, MN, USA), biodegradable polylactide (PLA), polyglycolide (PGA), polycarbonate and collagen (Inion®, Inion Oy, Tampere, Finland), Guidor® (Guidor AB, Huddinge, Sweden) and BioGide® (Geistlich Pharma AG, Wolhusen, Switzerland)). Although present polymeric products show positive results in clinical studies, their weak mechanical properties and poor bone regeneration capacity are still major challenges. To overcome these problems, recent research efforts have included the incorporation of bone-like ceramics into the membranes, e.g. hydroxyapatite, tricalcium phosphate and calcium carbonate [4–6]. In these efforts, nano-sized ceramic

* Corresponding author. Tel.: +31 24 3614006; fax: +31 24 3624657.
E-mail address: J.Jansen@dent.umcn.nl (J.A. Jansen).

1742-7061/$ - see front matter © 2009 Acta Materialia Inc. Published by Elsevier Ltd. All rights reserved.
doi:10.1016/j.actbio.2009.05.023

particles are of particular interest as they mimic the mineral crystals as present in the natural tissue and have been shown to induce a significant increase in protein absorption and cell adhesion, compared to their micro-sized counterparts [7,8].

Although numerous membrane materials have been investigated, few studies have focused on the technique of membrane preparation. So far, most GTR/GBR membranes are made in the shape of porous foam, created by traditional methods such as particulate leaching, solvent casting or gas foaming [9,5]. Recently, a new technique has been introduced, which is called electrospinning, and allows the preparation of thin fibrous membranes [6,10]. Electrospinning makes use of a high electric voltage to draw polymer solutions/melts into a whipped jet, which becomes ultrafine fibers after drying in air [11]. Fibers obtained from electrospinning are in the range of 50 nm to a few microns in diameter and generally collected in the form of a non-woven structure. It has already been shown that electrospun membranes have the potential to promote osteoblastic cell function and bone regeneration [11,12]. More importantly, the pore size of the electrospun membranes in general is less than the average cell size, and previous studies have shown that such small pores do not allow cell penetration [13,14].

In view of the above mentioned, the aim of the current study was to develop a composite GTR/GBR membrane containing nano-apatite (nAp) particles and biodegradable poly(ε-caprolactone) (PCL) fibers by electrospinning, and to test the mechanical properties, bioactivity and osteoblast-like cellular behavior in vitro. In order to study the effect of nAp, three membranes with different nAp content were chosen. Our hypothesis was that electrospinning is a suitable method to fabricate GTR/GBR membranes; and that the addition of nAp improves the properties of polymeric membranes in the aforementioned terms, especially the mechanical properties and the bioactive behavior.

2. Materials and methods

2.1. Preparation of nano-apatite particles

Nano-apatite (nAp) was synthesized following a precipitation reaction. In brief, 0.3 M orthophosphoric acid (H_3PO_4) (Acros Organics, Geel, Belgium) was added drop-wise to a 0.5 M calcium hydroxide ($Ca(OH)_2$) (Mallinckrodt Baker, Phillipsburg, NJ, USA) suspension under continuous stirring overnight at room temperature, while the pH was kept above 10.5 by the addition of ammonia solution. Then, the obtained precipitate was aged for one week at room temperature and centrifugal washing with deionized water three times. After each washing step, an ULTRA-TURRAX® homogenizer (T25, IKA® Werke, Staufen, Germany) was used to re-suspend the particles. Finally, the resultant was freeze-dried to obtain very fine particles, thereafter named nAp.

To observe the morphology of the obtained particles, one drop of an aqueous dispersion of nAp was put on a Formvar-coated copper grid and air-dried at room temperature. The dried grid was examined by transmission electron microscopy (TEM; JEOL 1101, Tokyo, Japan). The crystallographic structure of the particles was verified by X-ray diffraction (XRD) using a θ–2θ X-ray diffractometer (PW3710, Philips, Eindhoven, The Netherlands) with Cu K_α radiation (45 kV, 40 mA). The scanning range was from 20 to 40° with a step size of 0.02°. The chemical structure of the particles was examined using Fourier transform infrared spectrometry (FTIR, Spectrum One, Perkin-Elmer, Waltham, MA, USA) with an attenuated total reflection (ATR) accessory.

2.2. Fabrication of membranes

Membranes were fabricated using the electrospinning technique. The electrospinning dope without nAp was prepared from poly(ε-caprolactone) (PCL, $M_n = 80{,}000$, Sigma). PCL was dissolved in 80% 2,2,2-trifluroethanol (TFE) (Acros Organics, Geel, Belgium) in deionized H_2O at a concentration of 12% w/v. For the electrospinning dope containing nAp, a defined amount of nAp was suspended in the solvent by ultrasonic and vigorous stirring before adding the polymers. Dioctyl sulfosuccinate sodium salt (0.05% w/v) was used as a surfactant and dissolved in the solvent to obtain stable particle suspension in the polymer solution. Three types of membranes were prepared and named n0, n25 and n50 based on the amount of nAp in the membranes. Their detailed composition is listed in Table 1. Note that the solvent for n0 was 80% TFE in phosphate buffer saline (PBS) as a preliminary study showed that one could not obtain uniformed fibrous structure when using 80% TFE in H_2O as solvent.

A commercially available electrospinning set-up (Advanced Surface Technology, Bleiswijk, The Netherlands) was used for the scaffold fabrication, as described previously [15]. Briefly, 10 ml of the prepared dope was fed into a syringe, which was controlled by a syringe pump (KD Scientific Inc., Holliston, MA, USA) at a feeding rate of 2 ml h^{-1}. A Teflon tube was used to connect the syringe and a blunt-end nozzle with an inner diameter of 0.5 mm, which was set up vertically. The distance between the nozzle and a grounded collector was adjusted to 12 cm. A high voltage of 18–22 kV was applied to generate a polymer jet. On the basis of a pilot study, the processing parameters were chosen such that uniform fibrous structures were formed. The resulting fibers were collected on a rotating mandrel, left in vacuum conditions overnight to eliminate solvent residues and then kept in a desiccator for further experimentation.

The morphology of the fabricated membranes was observed by scanning electron microscopy (SEM; JEOL 6310, Tokyo, Japan) and TEM. The TEM samples were prepared by directly depositing the as-spun fibers onto the Formvar-coated copper grids. The fiber diameters were measured from SEM micrographs obtained at random locations ($n = 50$). Pore size distribution of each membrane

Table 1
The compositions of 10 ml electrospinning dopes and the obtained fiber size.

Sample	n0	n25	n50
PCL (g)	1.2	1.2	1.2
nAp (g)	0	0.3	0.6
PCL:nAp			
Theoretical	100:0	100:25	100:50
Actual (TGA results)	100:0.0	100:25.6	100:46.2
Diocty sulfosuccinate sodium salt (mg)	0	5.0	5.0
Solvent	80% TFE in PBS	80% TFE in H_2O	80% TFE in H_2O
Obtained fiber diameter (μm)	0.32 ± 0.13	0.39 ± 0.22	0.43 ± 0.25
Pore size (μm)			
Major axis	1.14 ± 0.51	0.92 ± 0.38	1.61 ± 1.02
Minor axis	0.51 ± 0.26	0.46 ± 0.21	0.69 ± 0.45

was estimated using an image analysis method by the software Image J (National Institutes of Health, Bethesda, MD, USA) from the SEM micrographs. In brief, the threshold function was used to separate the pore area from the whole image. Then the analyze particles function was applied in order to calculate the major/minor axis of individual pores. Only pores bigger than 0.1 μm^2 were counted due to the resolution of the images. For each membrane, two SEM micrographs were used and more than 1000 pores were analyzed.

To determine the actual content of nAp in the composite membrane, thermogravimetric analysis (TGA) was carried out from room temperature to 600 °C by using a TGA instruments Q500 (New Castle, DE, USA) under a N_2 atmosphere at a heating rate of 10 °C min^{-1}. XRD and FTIR spectrometry were used to observe the crystal and chemical structure of the membranes.

2.3. Mechanical characterization

The fabricated membranes were carefully cut into rectangular shapes of 10 mm in width and 50 mm in length. The thickness of the membranes was measured with a micrometer having a precision of 0.01 mm. Tensile test was conducted on a MTS 858 Mini Bionix II test system (Eden Prairie, MN, USA) equipped with a 250 N load cell under a cross-head speed of 10 mm min^{-1}. The gauge length of the samples was set at 40 mm. Tensile stress (σ) was calculated based on the apparent cross-sectional area of the membranes. Six samples were tested for each type of membrane.

The following mechanical properties were recorded or calculated from the stress–strain (σ–ε) curves: (1) the tensile modulus was calculated from the slope of the initial linear part of the curve, (2) the strain at break was defined as the maximum strain that the samples could reach, and (3) the energy per volume was expressed by the area under the σ–ε curve.

2.4. Simulated body fluid (SBF) immersion test

The recipe for the preparation of SBF was adopted from Kokubo [16,17]. The pH value of the solution was adjusted to 7.4 after complete preparation. Immersion studies were performed by incubating a membrane (disk shape with a diameter of 15 mm) in 10 ml SBF solution in a 15 ml tube. Three samples were used for each condition. All tubes were placed in a water bath at 37 °C under continuous shaking. After immersion periods of 2 and 4 weeks, the membranes were gently washed with deionized water and freeze-dried. The membranes were then sputter-coated with gold and their morphology was examined by scanning electron microscopy.

2.5. Cell isolation, seeding and culture

Before cell seeding, all experimental membranes (disk shape with a diameter of 15 mm) were pre-wetted and sterilized in 70% ethanol for 2 h and subsequently washed by PBS twice. Then they were transferred into 24-well plates and soaked in the culture medium overnight before cell seeding.

Rat bone marrow (RBM) cells were isolated from femora of male Wistar rats of 40–43 days after approval from the Radboud University Nijmegen Animal Ethics Committee (RU-DEC 2004-156). The femora were excised aseptically and washed three times in α-MEM (Minimal Essential Medium; MEM Gibco BRL, Life Technologies BV, Breda, The Netherlands) supplemented with 0.5 mg ml^{-1} gentamycin and 3 μg ml^{-1} fungizone. Subsequently the epiphyses of the femora were removed and the diaphyses were flushed out with 30 ml culture medium, i.e. α-MEM supplemented with 10% FCS (fetal calf serum, Gibco), 50 μg ml^{-1} ascorbic acid (Sigma, St. Louis, MO, USA), 50 μg ml^{-1} gentamycin, 10 mM Na β-glycerophosphate (Sigma) and 10^{-8} M dexamethasone (Sigma). Cells were incubated at 37 °C, 95% humidity and 5% CO_2. The medium was changed every 2 or 3 days.

After 1 week of primary culture, the RBM cells were detached using trypsin/EDTA (0.25% w/v trypsin/0.02% EDTA). Cells were seeded onto the membranes at a density of 2×10^4 cells cm^{-2}, and then cultured for 1, 4, 8, 16 and 24 days while the medium was changed every 2 or 3 days.

2.6. DNA analysis and alkaline phosphatase (ALP) activity

To assess the proliferation rate of the cells, total DNA content ($n = 3$) was measured by a PicoGreen dsDNA

quantification kit (Molecular Probes, Leiden, The Netherlands) as described previously [18]. Briefly, after washing twice in PBS, each membrane was transferred to a tube and 1 ml of deionized water was added to lyse the cells. Thereafter, the cell–membrane complexes together with the 1 ml water were subjected to a freeze–thaw cycle and sonicated for 15 min. Then, 100 μl of PicoGreen working solution was added to 100 μl of supernatants of the samples. Subsequent to 2–5 min of incubation, the DNA was measured on a fluorescence microplate reader (Bio-Tek Instruments Inc., Winooski, VT, USA), with excitation of 265 nm and emission of 450 nm, and the DNA amounts were calculated from a standard curve.

The same supernatants of the samples as used for DNA assay were also used to measure the ALP activity ($n = 3$). To perform the measurement, 20 μl of 0.5 M 2-amino-2-methyl-1-propanol (AMP) buffer (Sigma) was added to 80 μl of the samples or standards. Next, 100 μl of substrate solution prepared from p-(nitrophenyl phosphate) was added and the mixtures were incubated at 37 °C for 1 h. The ALP activity was measured at 405 nm using an ELISA microplate reader (Bio-Tek Instruments Inc., Winooski, VT, USA).

2.7. Scanning electron microscopy for cell morphology

On days 4 and 16 after cell seeding, cell–membrane complexes ($n = 2$) were washed in PBS twice and fixed in 2% glutaraldehyde for 15 min. Then, the samples were dehydrated in graded series of ethanol and air-dried in tetramethylsilane (Merck, Darmstadt, Germany). After gold sputtering, the specimens were examined by SEM.

2.8. Statistical analysis

Statistical significance in this study was evaluated using a one-way ANOVA with a post hoc Tukey test. Differences were considered statistically significant at $p < 0.05$.

3. Results

3.1. Characterization of nAp particles

A representative TEM micrograph of the obtained nAp particles is depicted in Fig. 1a. The particles showed a rod-like appearance with a length and width of around 60 and 20 nm, respectively. Further, XRD and FTIR spectrometry were used to identify the crystallographic and chemical structure of the particles (Fig. 2a and b). The XRD pattern indicated the Bragg peaks appearing approximately at 25.9°, 31.8°, 32.9° and 34.1° in 2θ, which corresponded to the characteristic reflections of 002, 211, 300 and 202 of an apatite structure. The FTIR spectrum bands at 962 ($\nu 1$), 1026 and 1092 ($\nu 3$), 563 and 603 ($\nu 4$) cm^{-1} were assigned to PO_4^{3-} and the one at 3384 cm^{-1} was attributed to O–H stretching. In addition, CO_3^{2-} was recorded by weak bands at 876, 1420 and 1473 cm^{-1}, suggesting a small amount of CO_3^{2-} ions in the apatite structure.

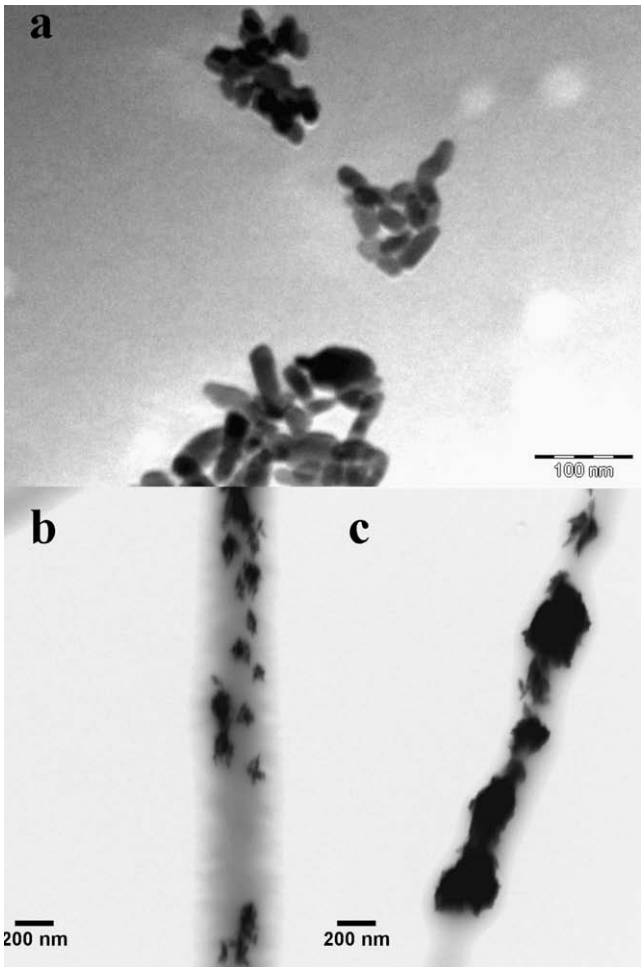

Fig. 1. Transmission electron micrograph of (a) nAp particles, (b) fiber n25, and (c) n50.

3.2. Characterization of membranes

The TEM micrographs demonstrated that the nAp particles were dispersed in the polymer fibers (Fig. 1b and c). Fiber n50 showed more nAp particles, thus was thicker than fiber n25. SEM micrographs revealed that all the electrospun membranes were composed of randomly oriented fibers (Fig. 3). The nAp particles were distributed evenly through the material. Visual inspection evidenced that most particles were embedded in the fibers, while some seemed exposed to the fiber surface (Fig. 3b and c). The size of the fibers was measured from the micrographs and is listed in Table 1. As expected, the addition of nAp increased the fiber diameter. The pores within the membranes greatly differed in size due to the random orientation and interconnection of the fibers, but in general the pore size was smaller than 2 μm (Table 1). The true content of nAp in the membranes was evaluated by TGA and the results are shown in Table 1.

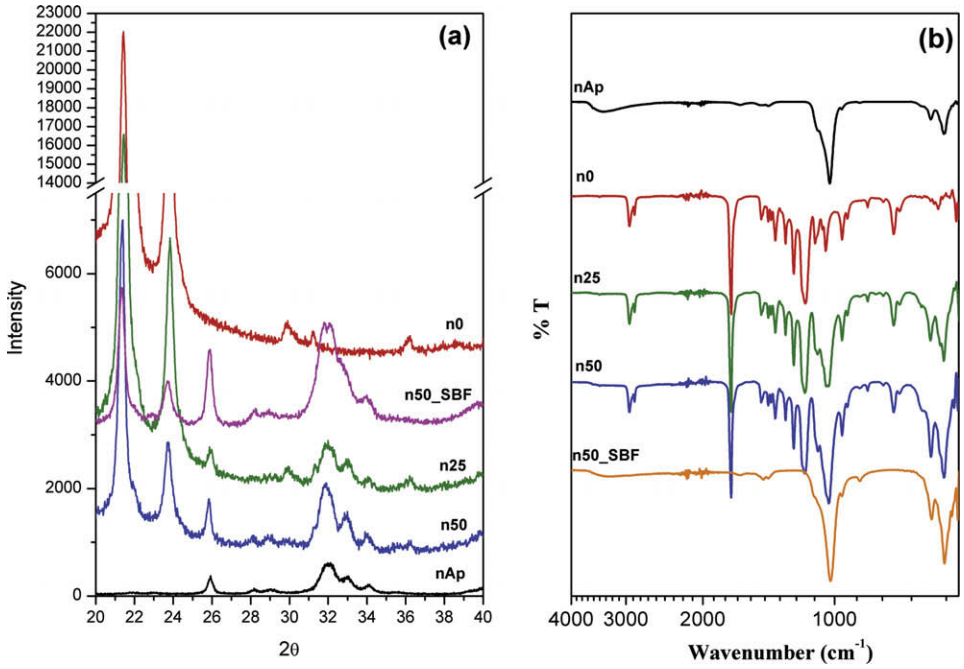

Fig. 2. (a) XRD and (b) FTIR spectra of nAp particles, electrospun membranes (n0, n25, and n50) and n50 immersed in SBF for 4 weeks.

The XRD patterns of the different membranes are depicted in Fig. 2a. The n0 membrane, prepared from PCL, displayed two very intensive and sharp peaks at 21.4° and 23.8° 2θ and three week peaks at 29.8°, 31.2° and 36.2°. The n25 composite membrane from PCL and nAp exhibited peaks from both materials. Besides showing weakened PCL peaks, characteristic peaks of nAp were seen at 25.9°, 31.8°, 32.9° and 34.1°. With the increased ratio of nAp, the n50 composite membrane showed more intensive nAp peaks, while those at 21.4° and 23.8° representing PCL were less intensive when compared to n25. In addition, the peaks at 29.8°, 31.2° and 36.2° had disappeared.

The corresponding FTIR spectra of the membranes are shown in Fig. 2b. When comparing the spectra of the two composite membranes with the control n0 membrane, it was seen that the PO_4^{3-} absorbance emerged at the 950–1100 and 550–620 cm^{-1} ranges. Further, the intensity of

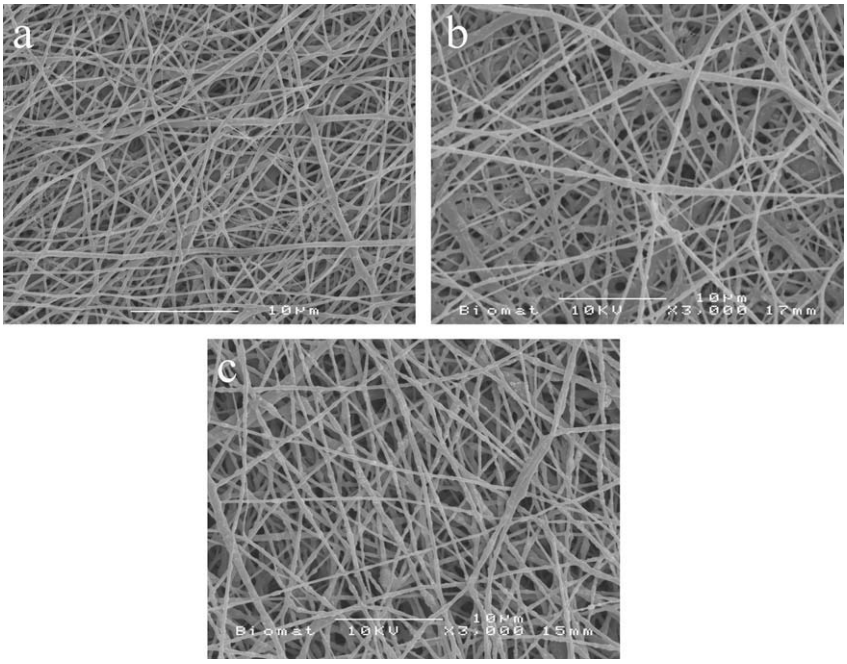

Fig. 3. Scanning electron micrographs of the three electrospun fibrous membranes: (a) n0; (b) n25; and (c) n50.

these absorbance bands increased with the increasing weight ratio of nAp.

3.3. Mechanical test

Fig. 4 shows the typical stress–strain curves for the electrospun membranes. They exhibited similar mechanical behavior under tensile force, as is characteristic for ductile materials. In the beginning of the curves (strain < 10%), the membranes obeyed Hooke's law, showing a proportional increase of stress and strain. As strain continuously increased, the curves deviated from the linear proportionality. The mechanical properties recorded or calculated from the curves are listed in Table 2. With the addition of nAp, the tensile modulus, strain at break and energy per volume of the membranes increased significantly ($p < 0.001$). The n25 membrane showed the highest value among all samples ($p < 0.001$, except for strain at break, $p < 0.01$).

3.4. SBF immersion test

There was no CaP precipitation visible on membrane n0 in SBF solutions up to 4 weeks of incubation (results not shown). However, for the n25 composite membrane, tiny needle-like CaP depositions could be seen on the fiber surface (Fig. 5a). These needle-like CaP depositions became more obvious when the immersion period reached 4 weeks (Fig. 5b). The CaP deposition process on n50 membrane went much faster. After 2 weeks, the fibers were partially covered by a needle-like CaP precipitation (Fig. 5c). After 4 weeks of immersion, all fibers were fully covered by a layer of nano-textured cauliflower-like CaP coatings (Fig. 5d). The CaP nature of all the deposits was confirmed by XRD and FTIR. Fig. 2 shows the spectrum of n50 immersed in SBF for 4 weeks, which also indicated that the obtained CaP coating was a low crystalline apatite, with similar composition and structure to the incorporated nAp.

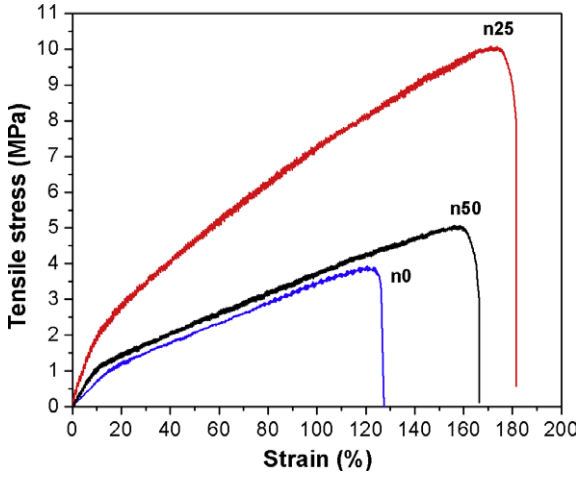

Fig. 4. Typical tensile stress–strain curves of the electrospun membranes.

Table 2
Mechanical properties of the electrospun membranes.

Sample	Modulus (MPa)	Strain at break (%)	Energy per volume (N mm/mm^3)
n0	6.77 ± 0.31	121 ± 13	2.69 ± 0.47
n25	19.46 ± 0.97	196 ± 14	10.66 ± 0.23
n50	13.46 ± 1.29	161 ± 15	5.62 ± 0.74

3.5. Cell proliferation and differentiation analysis

The data from the DNA assay are shown in Fig. 6a. The DNA content found on all three different membranes increased gradually until day 24. Until day 8, there were no significant differences among the DNA content for all membranes, but on day 24 a greater DNA content was found for n0 compared to n50.

The results of the ALP activity measurements are depicted in Fig. 7b. The expression of ALP activity was about the same from day 1 to day 8, but increased on day 16 and then significantly decreased on day 24. The cells on both composite membranes showed significantly higher levels of ALP compared to those cultured on the pure polymer membrane n0 at days 1, 4 and 8. After day 16, no significant differences in the ALP expression were found.

3.6. Cell morphology

Upon visual inspection the fibrous morphology of all the membranes retained unaltered for the 16-day culturing period. On day 4, cells adhered well and spread similarly on the surfaces of all the membranes (Fig. 7a, c, and e). Due to the small pore size of the membranes, cells remained on the surface. The cells showed obvious proliferation towards day 16 (Fig. 7b, d, and f). More cells could be found on n0 than on n25 and n50.

4. Discussion

In this study, we have successfully fabricated nano-sized calcium phosphate particles using a wet chemical deposition method. The XRD and FTIR results indicated that the nAp was composed of a poorly crystallized apatite phase containing CO_3^{2-}, i.e. a similar structure as the mineral phase of natural dentin and bone [19]. The nAp particles were mixed with PCL polymer and fabricated into composite membranes using the electrospinning technique. The composite membranes consisted of continuous submicron fibers with nAp dispersed inside. The fine fibrous structure resulted in a large surface area-to-volume ratio and interconnected porosity. These factors are considered essential for cellular growth in vitro and in vivo as they are directly involved in the transport of oxygen and nutrients to the cells [20]. By varying the polymer solution properties and electrospinning processing parameters, e.g. polymer concentration, solvent, applied voltage, feeding rate, electrospun fibers with different diameters ranging

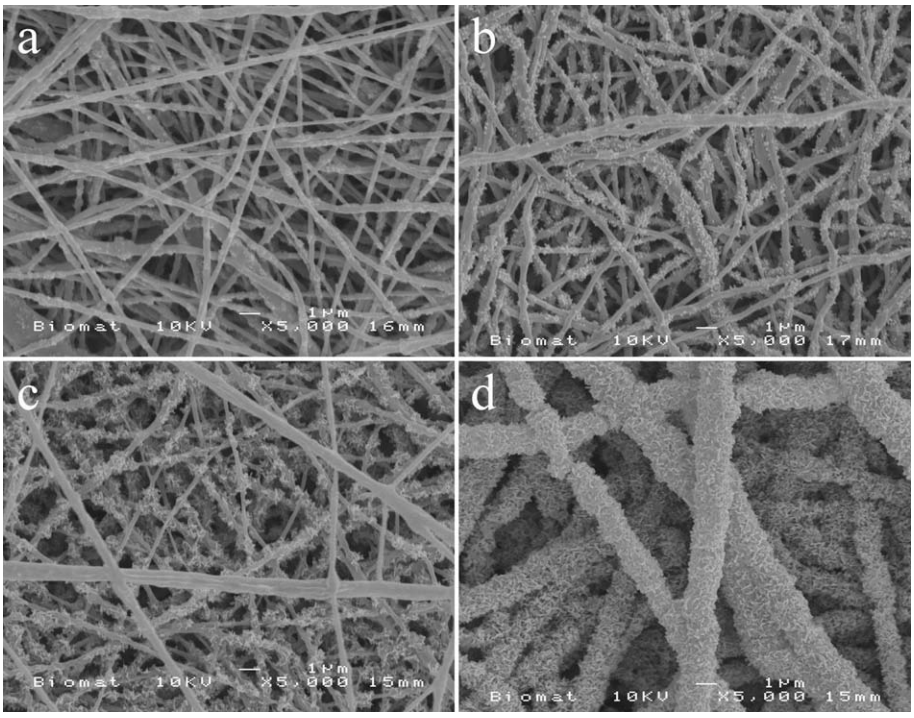

Fig. 5. Scanning electron micrographs of the composite electrospun membranes after SBF immersion: (a) n25 for 2 weeks; (b) n25 for 4 weeks; (c) n50 for 2 weeks; and (d) n50 for 4 weeks.

from tens of nanometers to 10 μm can be prepared as well as membranes with different pore sizes [13,20]. To choose a suitable pore size for the membranes is of utmost importance for our specific application. A GBR/GTR membrane should contain small pores at one side of the membrane to prevent the fast-growing connective tissue and epithelial cells from migrating into the wound and big pores at the other side, which favor bone tissue growth and integration. This requirement can be easily fulfilled when designing double-layer structures using the electrospinning technique.

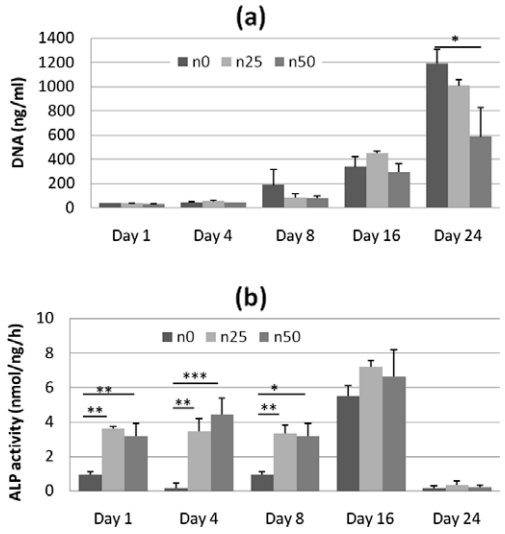

Fig. 6. (a) DNA content and (b) ALP activity of osteoblast-like cells cultured on the electrospun membranes. The bars represent the mean ± SD ($n = 4$). The significant difference is shown as $^{*}p < 0.05$, $^{**}p < 0.01$, and $^{***}p < 0.001$.

In surgery, GBR/GTR membranes are tightly fixed by biodegradable pins, medical glue or sutures preventing them from sagging into bone defects [6]. Our mechanical test showed that the addition of nAp increased the mechanical properties of the PCL membrane. Among the three membranes that we tested in this study, the n25 showed the highest tensile strength, ductibility and toughness. With an increasing nAp content, the n50 showed weakened properties compared with n25, but remained stronger and tougher than the pure PCL membrane n0. This mechanical reinforcement effect can be attributed to an additional energy-dissipating mechanism introduced by the nanoparticles in PCL. Recent molecular dynamics studies suggested that this additional dissipative mechanism is a result of the mobility of the nanoparticles. During the deformation process the nanoparticles orient and align under tensile stress, creating temporary cross-links between polymer chains, thereby creating a local region of enhanced strength [21]. However, when the size of the nAp stacks is increased, as in the n50, they become less mobile. Therefore, the ability of the nAp to dissipate energy is also reduced, resulting in almost no improvement in the toughness of the material. Our results are consistent with a previous study [22], yet another report showed that the addition of nano-sized calcium carbonate weakened the PCL membrane [6]. This discrepancy can be due to a difference in dispersion of particles. In order to achieve a stable and uniform nAp suspension in the polymer solutions, the surfactant, dioctyl sulfosuccinate sodium salt was used in the present study.

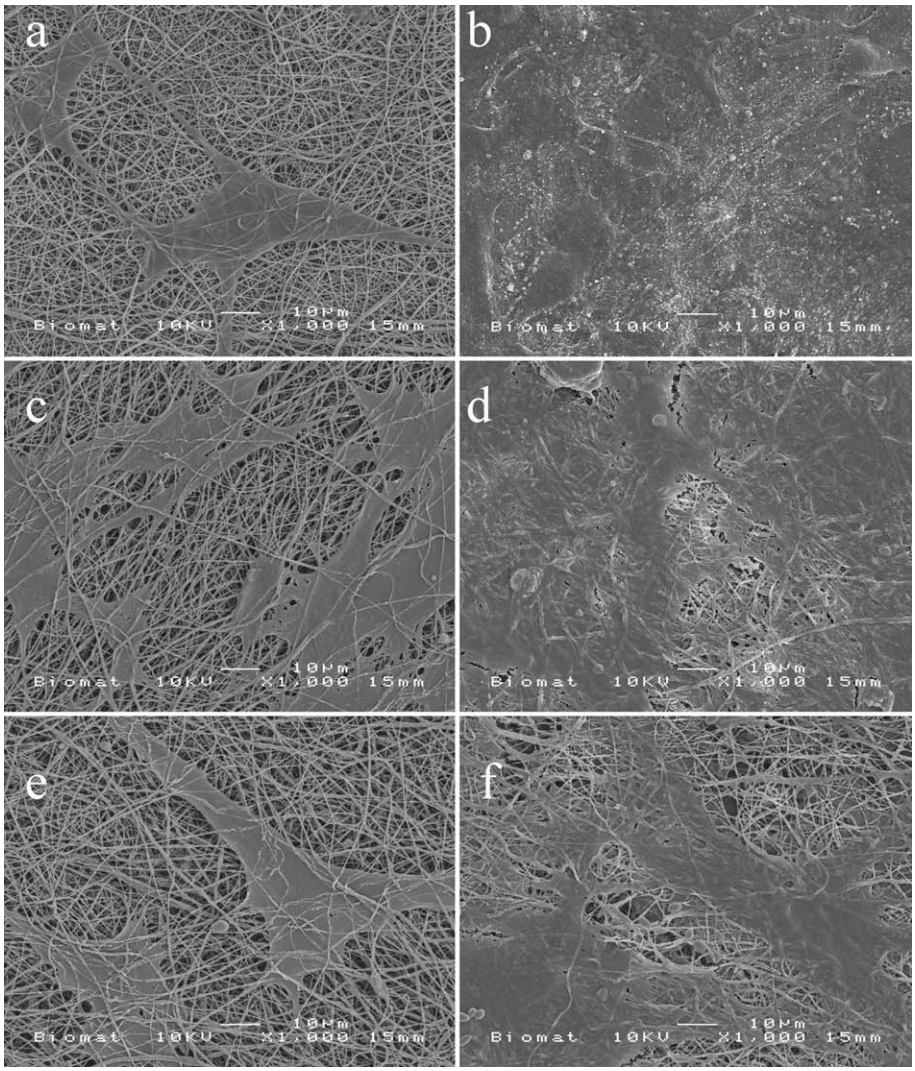

Fig. 7. Scanning electron micrographs of rat bone marrow cells cultured on different groups of membranes: (a) n0, (c) n25, and (e) n50 for day 4; (b) n0, (d) n25, and (f) n50 for day 16.

The concept of using a surfactant was brought forward by Kim and co-workers, who used oleic acid as an amphiphilic surfactant to mediate the interaction between the hydrophilic hydroxyapatite (HA) and hydrophobic PCL [23,24]. Such uniformly distributed HA particles also resulted in a higher mechanical strength compared with conventional composite and the pure PCL [23].

Besides mechanical properties, the bone-forming ability is another important characteristic. The bone-forming ability of a material is evaluated by examining the ability of apatite formation on its surface by incubation of the material in SBF with ion concentrations equal to human blood plasma [16]. Apatite formation does not occur spontaneously on most synthetic polymers without pretreatment to activate their surfaces [25–28]. This corresponds to our result that there was no apatite formation on the PCL membrane after 4 weeks. The incorporation of nAp promoted precipitation on the fibers, which can be attributed to: (i) the partial dissolution of nAp and the subsequent release calcium ions, which favors apatite formation, and/or (ii) the exposure of nAp particles on the PCL surface provides nucleation sites for apatite formation or growth [25].

Also, the behavior of osteoblast-like cells on the surface of the different membranes was studied in terms of cell proliferation and differentiation. Despite previous studies reporting a beneficial effect of calcium phosphate on osteoblast-like cell proliferation [29,30], our DNA results indicated that there was no significant differences between the DNA content on each membrane up to 16 days of culture. In contrast, the composite surface showed lower cell numbers compared to the pure PCL surface after 24 days. Such lower cell numbers are probably the result of an earlier cell differentiation on the composite surface [31]. This was corroborated by our ALP activity results, which suggested an earlier differentiation for the cells on the apatite-incorporated surfaces. Our data are also consistent with other studies, which showed that hydroxyapatite provides a suitable environment for osteoblast-like cell differentiation [32,33].

The cell part of the study here was of limited size and in the future the membranes should be completely tested using different cell types, e.g. gingival fibroblasts, periodontal ligament fibroblasts and osteoblast-like cells in terms of cell attachment, proliferation, migration, penetration, differentiation and mineralization [34]. Nevertheless, our results thus far showed that the composite membrane provided a good prototype towards developing an optimal GTR/GBR system.

5. Conclusion

The optimal resorbable membrane for GTR or GBR has to be strong, able to stimulate bone formation and promote osteoblast-like cell proliferation and differentiation. In the present study, a composite fibrous membrane based on nAp and PCL was prepared by electrospinning. Physiochemical, mechanical and in vitro characterization showed that the composite membrane fulfilled all aforementioned requirements. However, the membrane with a high nAp loading density was weaker than the one with low nAp loading density. Based on our results, we conclude that the composite fibrous membrane prepared by electrospinning is suitable for the use as a GTR/GBR membrane and it is a useful prototype for further development of a final membrane for clinical use.

Acknowledgments

The authors thank Drs. Wouter Habraken and Joop Wolke for their help on the TGA and mechanical test. This work was supported by the Dutch Program for Tissue Engineering (DPTE) (Project No. NGT.6730) and the Royal Netherlands Academy of Arts and Sciences (KNAW; Project No. 04-PSA-M-02).

References

[1] Karring T, Nyman S, Gottlow J, Laurell L. Development of the biological concept of guided tissue regeneration—animal and human studies. Periodontol 2000 1993;1:26–35.
[2] Llambes F, Silvestre FJ, Caffesse R. Vertical guided bone regeneration with bioabsorbable barriers. J Periodontol 2007;78:2036–42.
[3] Park SH, Wang HL. Clinical significance of incision location on guided bone regeneration: human study. J Periodontol 2007;78:47–51.
[4] Schwarz F, Herten M, Ferrari D, Wieland M, Schmitz L, Engelhardt E, et al. Guided bone regeneration at dehiscence-type defects using biphasic hydroxyapatite + beta tricalcium phosphate (Bone Ceramic) or a collagen-coated natural bone mineral (BioOss Collagen): an immunohistochemical study in dogs. Int J Oral Maxillofac Surg 2007;36:1198–206.
[5] Liao S, Wang W, Uo M, Ohkawa S, Akasaka T, Tamura K, et al. A three-layered nano-carbonated hydroxyapatite/collagen/PLGA composite membrane for guided tissue regeneration. Biomaterials 2005;26:7564–71.
[6] Fujihara K, Kotaki M, Ramakrishna S. Guided bone regeneration membrane made of polycaprolactone/calcium carbonate composite nano-fibers. Biomaterials 2005;26:4139–47.
[7] Webster TJ, Ergun C, Doremus RH, Siegel RW, Bizios R. Enhanced osteoclast-like cell functions on nanophase ceramics. Biomaterials 2001;22:1327–33.
[8] Balasundaram G, Sato M, Webster TJ. Using hydroxyapatite nanoparticles and decreased crystallinity to promote osteoblast adhesion similar to functionalizing with RGD. Biomaterials 2006;27:2798–805.
[9] Nublat C, Braud C, Garreau H, Vert M. Ammonium bicarbonate as porogen to make tetracycline-loaded porous bioresorbable membranes for dental guided tissue regeneration: failure due to tetracycline instability. J Biomater Sci Polym Ed 2006;17:1333–46.
[10] Zhang S, Huang Y, Yang X, Mei F, Ma Q, Chen G, et al. Gelatin nanofibrous membrane fabricated by electrospinning of aqueous gelatin solution for guided tissue regeneration. J Biomed Mater Res A 2008 [Epub ahead of print].
[11] Pham QP, Sharma U, Mikos AG. Electrospinning of polymeric nanofibers for tissue engineering applications: a review. Tissue Eng 2006;12:1197–211.
[12] Shin M, Yoshimoto H, Vacanti JP. In vivo bone tissue engineering using mesenchymal stem cells on a novel electrospun nanofibrous scaffold. Tissue Eng 2004;10:33–41.
[13] Pham QP, Sharma U, Mikos AG. Electrospun poly(epsilon-caprolactone) microfiber and multilayer nanofiber/microfiber scaffolds: characterization of scaffolds and measurement of cellular infiltration. Biomacromolecules 2006;7:2796–805.
[14] Tuzlakoglu K, Reis RL. Biodegradable polymeric fiber structures in tissue engineering. Tissue Eng Part B Rev 2009;15:17–27.
[15] Yang F, Wolke JGC, Jansen JA. Biomimetic calcium phosphate coating on electrospun poly(ε-caprolactone) scaffolds for bone tissue engineering. Chem Eng J 2008;137:154–61.
[16] Kokubo T, Takadama H. How useful is SBF in predicting in vivo bone bioactivity? Biomaterials 2006;27:2907–15.
[17] Kokubo T, Hanakawa M, Kawashita M, Minoda M, Beppu T, Miyamoto T, et al. Apatite formation on non-woven fabric of carboxymethylated chitin in SBF. Biomaterials 2004;25:4485–8.
[18] Zhang W, Walboomers XF, Wolke JG, Bian Z, Fan MW, Jansen JA. Differentiation ability of rat postnatal dental pulp cells in vitro. Tissue Eng 2005;11:357–68.
[19] LeGeros RZ. Calcium phosphates in enamel, dentin and bone. Calcium phosphates in oral biology and medicine. Basel: Karger; 1991. p. 108–29.
[20] Murugan R, Ramakrishna S. Nano-featured scaffolds for tissue engineering: a review of spinning methodologies. Tissue Eng 2006;12:435–47.
[21] Shah D, Maiti P, Jiang DD, Batt CA, Giannelis EP. Effect of nanoparticle mobility on toughness of polymer nanocomposites. Adv Mater 2005;17:525–8.
[22] Thomas V, Jagani S, Johnson K, Jose MV, Dean DR, Vohra YK, et al. Electrospun bioactive nanocomposite scaffolds of polycaprolactone and nanohydroxyapatite for bone tissue engineering. J Nanosci Nanotechnol 2006;6:487–93.
[23] Kim HW. Biomedical nanocomposites of hydroxyapatite/polycaprolactone obtained by surfactant mediation. J Biomed Mater Res A 2007;83:169–77.
[24] Kim HW, Lee HH, Knowles JC. Electrospinning biomedical nanocomposite fibers of hydroxyapaite/poly(lactic acid) for bone regeneration. J Biomed Mater Res A 2006;79:643–9.
[25] Kokubo T. Apatite formation on surfaces of ceramics, metals and polymers in body environment. Acta Mater 1998;46:2519–27.
[26] Chen JL, Chu B, Hsiao BS. Mineralization of hydroxyapatite in electrospun nanofibrous poly(L-lactic acid) scaffolds. J Biomed Mater Res A 2006;79:307–17.
[27] Oyane A, Uchida M, Choong C, Triffitt J, Jones J, Ito A. Simple surface modification of poly(epsilon-caprolactone) for apatite deposition from simulated body fluid. Biomaterials 2005;26:2407–13.
[28] Oyane A, Uchida M, Yokoyama Y, Choong C, Triffitt J, Ito A. Simple surface modification of poly(epsilon-caprolactone) to induce its apatite-forming ability. J Biomed Mater Res A 2005;75:138–45.
[29] Chen Y, Mak AFT, Wang M, Li JS, Wong MS. In vitro behavior of osteoblast-like cells on PLLA films with a biomimetic apatite or apatite/collagen composite coating. J Mater Sci Mater Med 2008;19:2261–8.

[30] Venugopal J, Low S, Choon AT, Kumar AB, Ramakrishna S. Electrospun-modified nanofibrous scaffolds for the mineralization of osteoblast cells. J Biomed Mater Res A 2008;85:408–17.

[31] Malaval L, Liu F, Roche P, Aubin JE. Kinetics of osteoprogenitor proliferation and osteoblast differentiation in vitro. J Cell Biochem 1999;74:616–27.

[32] Ozawa S, Kasugai S. Evaluation of implant materials (hydroxyapatite, glass-ceramics, titanium) in rat bone marrow stromal cell culture. Biomaterials 1996;17:23–9.

[33] Yuasa T, Miyamoto Y, Ishikawa K, Takechi M, Momota Y, Tatehara S, et al. Effects of apatite cements on proliferation and differentiation of human osteoblasts in vitro. Biomaterials 2004;25:1159–66.

[34] Behring J, Junker R, Walboomers XF, Chessnut B, Jansen JA. Toward guided tissue and bone regeneration: morphology, attachment, proliferation, and migration of cells cultured on collagen barrier membranes. A systematic review. Odontology 2008;96:1–11.